



Analysis of Film Formation in High Chromium White Iron Hardfacing Alloys in Alkaline Solution using EIS and SIMS

Varmaa Marimuthu¹ · Poorwa Gore² · V. S. Raja² · Krishnan Kannoopatti¹

Received: 2 October 2017 / Revised: 23 April 2018 / Accepted: 3 June 2018 / Published online: 7 June 2018
© Springer International Publishing AG, part of Springer Nature 2018

Abstract

A popular hardfacing alloy consisting of high chromium white iron (HCWI) was deposited on low carbon steel using shielded metal arc welding. The wear-resistant alloys are not only used in applications requiring wear resistance but also used in applications involving fluids of a range of pH values. It is well known that chromium containing alloys have good corrosion resistance due to the presence of passive film. In this study for understanding the film formation on carbides and eutectic austenite matrix, HCWI alloy were exposed to potentials (0.157 V vs. SCE and 0.758 V vs. SCE) derived from potentiodynamic studies in highly alkaline solution of pH 14, simulating Bayer refining process in alumina industry. Electrochemical impedance spectroscopy (EIS) technique was used to analyse the impedance of films. The thickness and the composition of film properties at various potentials were investigated by time-of-flight secondary ion mass spectrometry (ToF-SIMS). At potential 0.157 V versus SCE, chromium carbide had a thick layer of oxide film consisting of mainly FeO with minor amounts of CrO. The eutectic austenite matrix consisted of a much denser and slightly thinner film of FeO. It is proposed in this study that for the formation of an oxide film on carbides, the carbides would have to dissociate on the surface. This dissociation of carbides may likely render the hardfacing alloy less effective in wear-resistant applications. The results were explained through superimposing the Pourbaix diagram of chromium carbides and iron (Fe).

Keywords Hardfacing · High chromium white irons · Alkaline · Passivity · ToF-SIMS · EIS · Pourbaix diagram of carbides

1 Introduction

Hardfacing alloys of high chromium white iron (HCWI) are used in the Bayer refining process in alumina industry to withstand wear in slurry pumps and pipelines. However, The Bayer process solution is highly alkaline with concentrated sodium hydroxide which causes severe corrosion of HCWI as well [1, 2]. There are only limited studies [1–5] done on the corrosion behaviour of HCWI in alkaline solutions with contrasting results. In some studies, HCWI consisting of ($\text{Cr}_7\text{C}_3 + \text{Cr}_3\text{C}_2$) primary, eutectic carbides, and eutectic austenite matrix when exposed to sodium hydroxide pH 14 was found to have the eutectic austenite matrix corroded in preference to carbides [1, 2, 4, 6]. Studies of Nelson [2]

and Mcleod [1] proposed that corrosion of eutectic austenite matrix occurred mainly due to depletion of chromium in the matrix. In contrast, Salasi [5] and Varmaa et al. [3] found that corrosion of HCWI occurred in primary and eutectic carbides rather than eutectic austenite matrix.

In the study conducted by Radhesh [7] on exposing HCWI in alkaline solution of 2 M NaOH through electrochemical impedance spectroscopy (EIS) found that HCWI hardfacing alloys showed high impedance values at higher anodic potential than the open circuit potential. It was proposed that the alloy had developed a film on its surface. The study conducted by Salasi et al. [8] on HCWI for analysing the passive oxide films using nano secondary ion mass spectrometry (NanoSIMS) in 0.2 M Na_2SO_4 solution found that thicker iron oxide (FeO) passive film formed on eutectic austenite matrix. The film on carbide was thinner than that on the matrix which was iron dominated.

Olsson et al. [9] found that solubility of chromium in stainless steel increases in alkaline solution. In other studies, Fajardo et al. [10] conducted passive film analysis using SIMS on low-nickel and AISI 304 austenitic stainless steels in

✉ Varmaa Marimuthu
varmaa.marimuthu@cdu.edu.au

¹ School of Engineering and IT, Charles Darwin University, Darwin, Australia

² Department of Metallurgical Engineering and Materials Science, IIT Bombay, Mumbai, India

highly alkaline solution and found that a duplex layer of passive film with domination of FeO in outer layer with rich CrO in the inner layer was formed. Iron element is stable in alkaline solution compared with chromium. Similar results were also proposed by other investigators on stainless steels in alkaline solution [11, 12].

Formation, and protective nature, of passive film due to chromium is well known. However, it was not clear how the formation of oxide film in HCWI affects the corrosion behaviour. Varmaa et al. [3] proposed that the formation of oxide film would result in the dissociation of chromium carbide albeit only on the surface. If the chromium carbides dissociate, it is likely that the hardfacing alloy will suffer more loss when subjected to erosion–corrosion. In this experimental study, the nature of oxide film on HCWI in alkaline environment and its effect on corrosion behaviour was investigated. It is hoped that this study will lead to development of better hardfacing alloys and protection methods for these alloys.

2 Experimental Method

The HCWI-based hardfacing alloys were deposited on low carbon steel using shielded metal arc welding. The typical chemical composition of the deposited hardfacing alloys is given in Table 1. The alloy, called 9E, mainly had high chromium and carbon contents which form primary carbides and eutectic carbide and austenitic matrix [13, 14]. The recommended welding parameters provided by the manufacturer of the hardfacing alloys are given in Table 2. After the welding was performed, samples were prepared from the weld deposits for microstructural observations. The samples were etched in 20 ml distilled water, 10 ml HCl, 30 ml HNO₃ and 5 g of FeCl₃ [15].

Electrochemical potentiostatic tests were conducted using a Gamry Reference 3000 potentiostat and a three-electrode cell. The 9E alloy (sample area=0.63 cm²) was the working electrode exposed to 2 M NaOH solution of pH 14 which was measured using a pH Cube. A platinum mesh (1 cm² area) and a saturated calomel electrode (SCE) were the counter and reference electrodes, respectively. Open circuit potential (OCP) was measured after stabilisation for 10 min, and then the potentiostatic tests were conducted at Potential 1 (0.157 V vs. SCE) and Potential 2 (0.758 V vs. SCE) in pH 14 [16]. Two potentials were selected based on previously published potentiodynamic polarisation data for this alloy [3]. These Potentials 1 and 2 are displayed on the regions of superimposed chromium carbide (Cr₇C₃)–iron (Fe) Pourbaix diagrams in Fig. 1 [3, 17]. Potential 1 in the potentiodynamic test was selected in the middle of a region where there was a slow

Table 2 Welding parameters used in the study

Welding type	Welding voltage (V)	Welding current (A)	Welding speed (mm/min)	Depositing numbers
SMAW	32 V	100–150 A	120–200 mm/min	4 layers, 5 beads

current increase with potential. Potential 2 was at a potential where the alloy corroded rapidly. After the potentiostatic tests, EIS tests were conducted at the OCP (–0.451 V vs. SCE) and at selected DC potentials (Potentials 1 and 2). The EIS tests are normally done at OCP but in this investigation EIS tests were conducted at two different potentials. It was anticipated that the true film behaviour may be ascertained if the tests were conducted at higher anodic potentials. The samples were polarised at these potentials and EIS tests were performed for 15 min by superimposing small amplitude of 10 mV ac voltage signals with a frequency ranging from 100 kHz to 0.01 Hz. The resulting impedance data were analysed using Echem Analyst software. The microstructure was examined using an optical microscope and scanning electron microscopy (SEM, Philips XL 30 series). Energy dispersive X-ray spectrometry (EDS) was used to study the chemical composition of samples held at different potentials. In order to ascertain the crystal structure of the constituents of the microstructures, the samples were investigated with X-ray PANalytical diffractometer (Empyrean) using Copper K_α X ray source.

The time-of-flight secondary ion mass spectrometer (ToF-SIMS) was used to determine the nature and depth of films on the samples at three different potentials. For depth profiling, 1 keV Cs⁺ ion beam was used to sputter 10×10 μm² crater area of the carbide and the eutectic austenite matrix phases separately for 300 s. These studies are likely to provide information on the thickness of surface film. A testing scheme is provided in Fig. 2.

3 Results and Discussion

3.1 Microstructural Characteristics of 9E Alloy

The microstructure of the weld deposit is as shown in Fig. 3. The SEM microstructure consisted of polygonal shaped chromium-rich primary carbides (a), eutectic carbides (b) and eutectic austenitic matrix (c). The extensive amount of hard chromium carbides and tough eutectic austenite matrix

Table 1 Chemical composition (wt%) of 9E alloy

Alloy type	C	Cr	Mn	V	Si	Ni	Mo	Fe
9E alloy	4.8	30.0	1.1	0.2	1.4	0.5	1.7	Bal

Fig. 1 Pourbaix diagram of Cr₇C₃-Fe in pH 14 with Potentials 1 and 2 of 9E sample [3, 17]

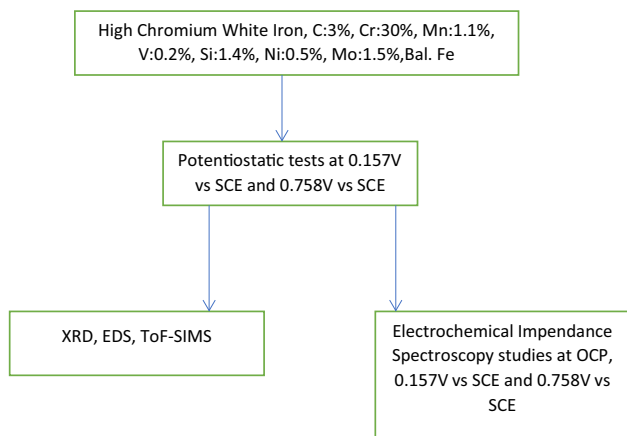
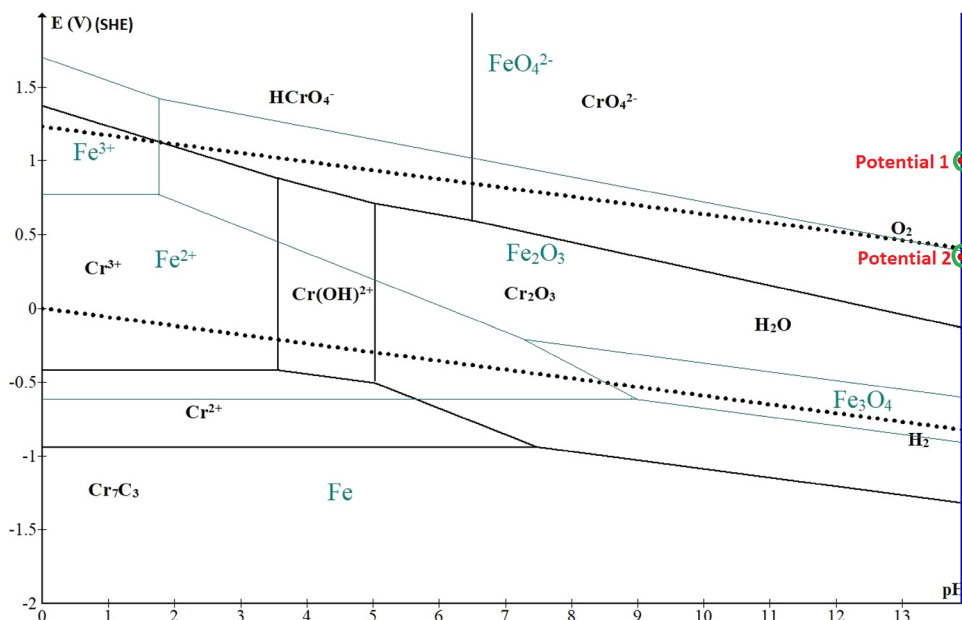


Fig. 2 Testing scheme for the research

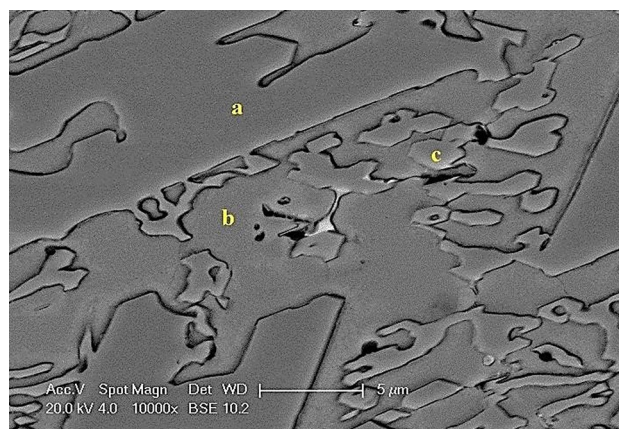


Fig. 3 SEM Microstructure of 9E sample showing polygonal **a** primary carbides surrounded by **b** austenite and **c** finer eutectic carbides

withstand granular abrasion at medium loads [14]. The formation of finer eutectic carbides (b) was seen adjacent to primary carbides (a) [18].

Elemental analysis of primary carbide which is shown in Fig. 3 is given Table 3. From Table 3, it can be seen that the carbides were predominantly made up of chromium and iron. Lazic et al. [19] reported that (Cr,Fe)₇C₃ alloy carbides were formed by dissolving chromium in cementite phase by substituting iron atoms. From the atom percentages in Table 3, it appears that the primary carbides could be Cr₃C₂. Other published works [13, 14] suggest that the primary carbides could be Cr₇C₃.

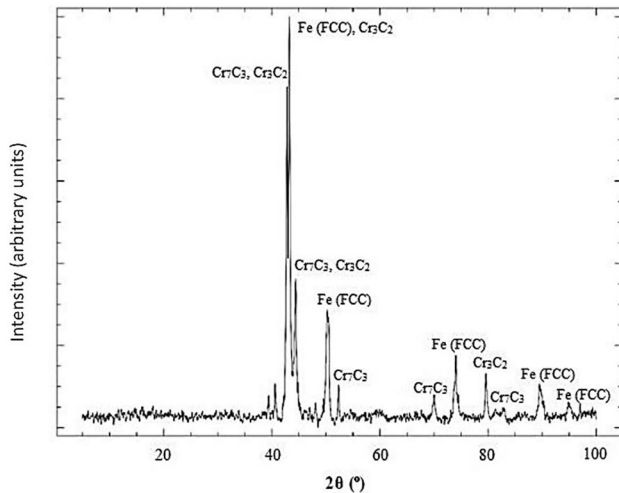
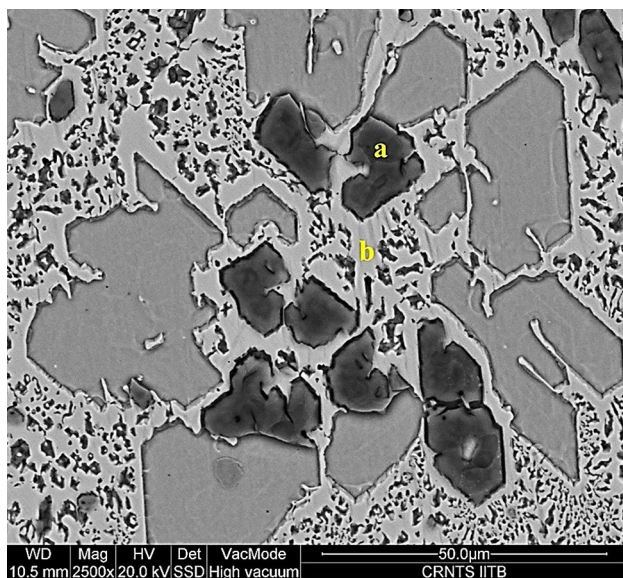
The X-ray diffraction results shown in Fig. 4 identified that the carbides were Cr₇C₃ and Cr₃C₂. Cr₃C₂ carbides were of high intensity in XRD pattern and these carbides are most likely primary carbides. It is possible that the eutectic

carbides could be Cr₇C₃. These carbon-rich chromium carbides (Cr₇C₃ and Cr₃C₂) are known to be stable at lower temperatures [20]. Literature available [13, 14] also nominate the matrix to be eutectic austenite and this was found to be the case from the X-ray diffraction results. Standard peaks for XRD for retained austenite and Cr₇C₃ are given in [21, 22].

The microstructure of the sample after the potentiostatic test at Potential 1 (0.157 V vs. SCE) in pH 14 solution is shown in Fig. 5. Corrosion occurred on eutectic and, partially, primary carbides. The eutectic austenite matrix (b) remains unattacked. Similar microstructures were shown by Varmaa et al. [3] on corrosion of HCWI in alkaline solution pH 14. In Table 4, EDS chemical analysis shows the presence of oxygen on the corroded carbides. The presence of oxygen suggests the possible formation of passive layer on

Table 3 EDS analysis of primary carbide for 9E sample

9E Alloy	Fe		Cr		C	
	(wt%)	(At. %)	(wt%)	(At. %)	(wt%)	(At. %)
Primary carbide (a)	38.20	24.47	47.38	32.59	14.42	42.94

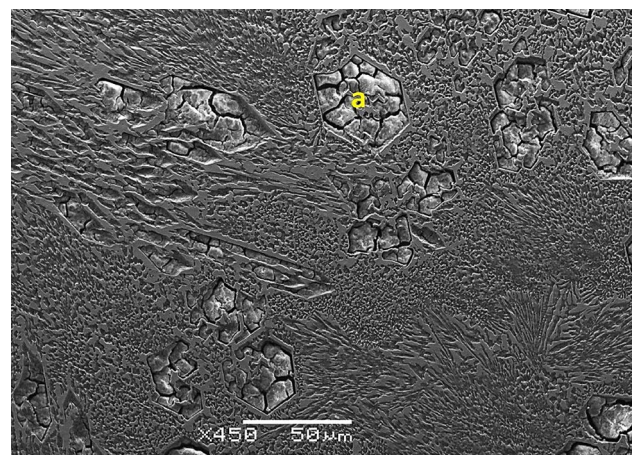
**Fig. 4** XRD pattern of 9E sample showing carbides (Cr_7C_3 and Cr_3C_2) and austenite (Fe FCC)**Fig. 5** SEM microstructure of corroded eutectic and partially corroded primary carbides (a) of 9E sample at 0.157 V versus SCE in pH 14 solution. (b) is eutectic austenite matrix which is unattacked

primary carbides. Chromium amounts in primary carbide have also reduced due to partial dissolution of carbides.

The microstructure of a sample after potentiostatic test at Potential 2 (0.758 V vs. SCE) in pH 14 solution

Table 4 EDS analysis (wt%) of corroded primary carbide for 9E sample at 0.157 V versus SCE in pH 14 solution

9E alloy at 0.157 V versus SCE	Fe	Cr	C	O
Corroded primary carbide (a)	45.56	15.86	15.58	23

**Fig. 6** SEM microstructure of corroded eutectic and primary carbides, a dissolved carbides of 9E sample at 0.758V versus SCE in pH 14 solution

is shown in Fig. 6. The potential is near the transpassive region of the potentiodynamic curve [3]. Eutectic and primary carbides were found to have corroded. The austenite eutectic matrix seems to be less attacked. Corroded carbides (a) in Fig. 6 show formation of cracks. Similar microstructures were obtained by Varmaa et al. [3] for HCWI in alkaline solution pH 14. A possible reason for the presence of cracks is due to the very brittle nature of carbides and the presence of high residual stresses due to welding. More work is necessary to investigate this. The significant drop in percentage of chromium in carbides shown in Table 5 is due to the instability of carbides at these potentials.

In summary, it was found that at both Potentials 1 and 2, eutectic and primary carbides corroded and the eutectic austenite matrix was less corroded. The EIS analysis of samples in pH 14 solutions at Potentials 1 and 2 will be discussed in following section.

Table 5 EDS analysis (wt%) of corroded primary carbide for 9E sample at 0.758V versus SCE in pH 14 solution

9E alloy at Potential 2	Fe	Cr	C	O
Corroded primary carbide (a)	48.91	2.18	18.52	30.40

3.2 EIS Analysis

Samples were first exposed to Potentials 1 and 2 and EIS tests were carried out at OCP (− 0.451 vs. SCE). Samples were also tested at Potential 1 (0.157 V vs. SCE) and Potential 2 (0.758 V vs. SCE) and Nyquist plots were produced. The Nyquist plots are given in Fig. 7. In Fig. 7a, b, Nyquist curves show capacitive arc between high and intermediate frequencies followed by an inductive arc at low frequencies for the specimen held at 0.157 V versus SCE. The capacitive arcs define the charge transfer processes as well as the resistance of the protective passive film that forms on the surface [23, 24]. The inductive loops can possibly be attributed to the formation of some intermediate species, which will be discussed later. In an earlier study by Varmaa et al. [3], the potentiodynamic curve did not display an ideal passive behaviour (potential independent current density region); instead it showed a gradual increase in current density with increase in potential. As the diameter of the capacitive arc of the samples exposed to Potential 1 (in the semi-passive region) is higher than that of the arcs of Potential 2 (in the transpassive region) it can be suggested that the presence of films on the surface is responsible for the high impedance value. Considering the microstructural variations shown by

the alloy held at the two different potentials as seen in Figs. 5 and 6, the Rp value of the specimen kept at Potential 2 in relation to that held at Potential 1 can be attributed to significant dissolution of carbides at these potentials making them difficult to repassivate [25]. The formation of inductive loop in Fig. 7a, b at low frequencies for samples exposed at Potential 1 is due to absorption of species from the electrolyte with slow changes in surface properties [24, 26]. The presence of inductive loop may be related to the presence of stable passive film on the surface [27, 28]. The diffusion element identified in the sample exposed to Potential 2 at low frequencies in Fig. 7b may be due continuous diffusion of corrosive species of electrolyte through the corroded products to the substrate [29].

3.3 ToF-SIMS analysis

ToF-SIMS depth profiles were recorded for understanding the films on carbide and eutectic austenite matrix of the sample exposed at Potentials 1 and 2 in pH 14 solution as shown in Figs. 8 and 9. Sputtering times are an indication of the thickness of films on the surface under depth profiling. Since the sputtering rates were not available, the profiles have not been converted to exact depth profiles. Also, since the ions detected in the spectra do not necessarily represent the state of species which exist in the oxide, the exact oxidation states of the ions could not be determined. Similar approach was also taken by Zang et al. [30, 31] as to the exact state of the oxides. Intensity values provide an indication of relative amounts of species present.

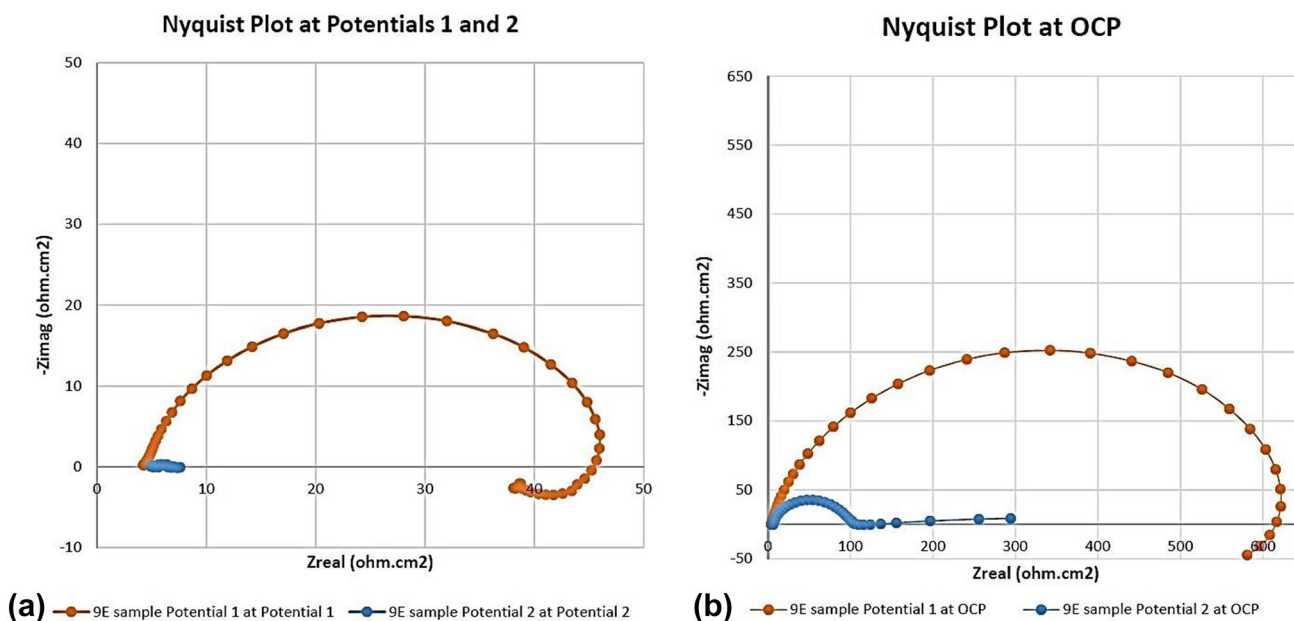


Fig. 7 Nyquist plots of **a** 9E samples held at Potentials 1 and 2 and **b** then obtained at OCP in pH 14 solutions

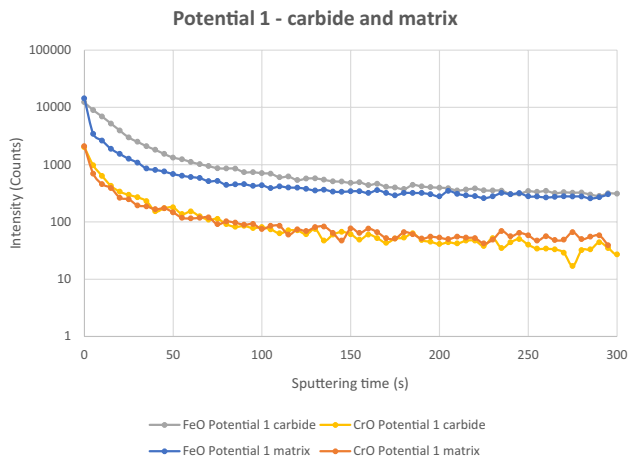


Fig. 8 ToF-SIMS depth profile of FeO and CrO for carbide and eutectic austenite matrix of 9E sample recorded at Potential 1 (0.157 V vs. SCE) in pH 14 solution

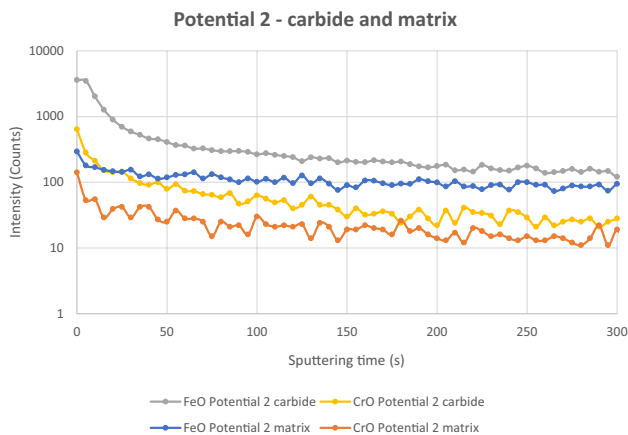


Fig. 9 ToF-SIMS depth profile of FeO and CrO for carbide and eutectic austenite matrix of 9E sample recorded at Potential 2 (0.758 V vs. SCE) in pH 14 solution

Figure 8 shows the depth profile of carbide and eutectic austenite matrix of samples at Potential 1 (0.157 V vs. SCE) in pH 14 solution, where the intensity of FeO in eutectic austenite matrix (14,331 counts) and carbide (12,311 counts) are significantly higher than CrO in eutectic austenite matrix (2090 counts) and carbide (2090 counts). The sputtering time to remove the FeO from the carbides was higher than from the matrix. This suggests that FeO on the carbides was thicker than on the eutectic matrix. However, in studies by Strehblow et al. [32, 33], Mcleod et al. [34] and Salasi [8] found that austenite matrix forms thicker and stable passive film than on primary carbide in highly alkaline solution. Hoppe et al. [33] stated that the dominance of FeO in passive layer is due to weak solubility of Fe species in alkaline solution. CrO layers are of lower intensity and are also thinner on both carbides and matrix as correlated to the sputtering

time to remove these layers. CrO was found to be also a part of the film where FeO dominated both in the carbides and eutectic austenite matrix. The higher intensity of FeO in eutectic austenite matrix is possibly due to a denser and a more uniform film on the austenite matrix.

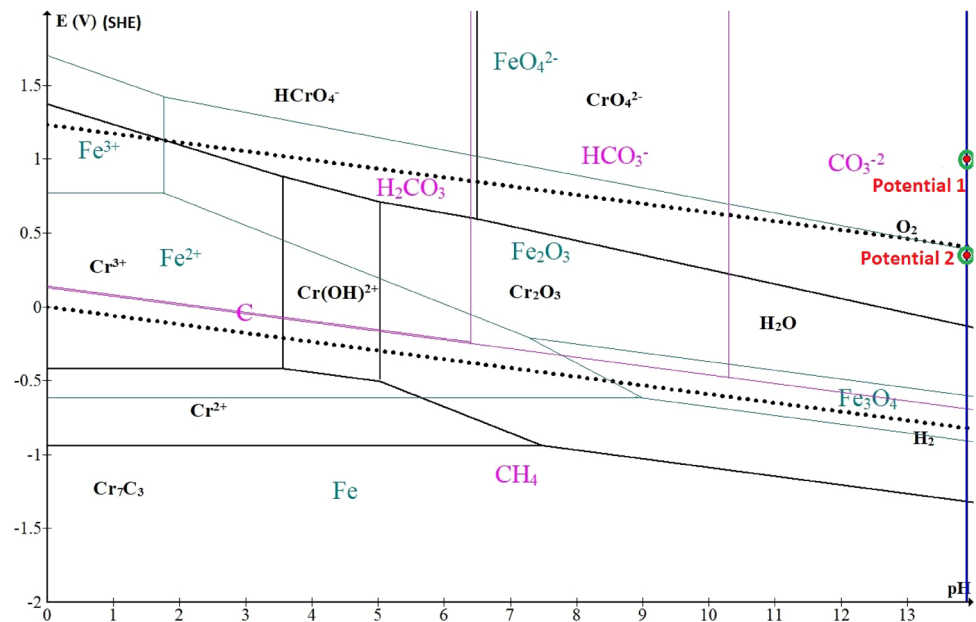
ToF-SIMS depth profile of carbide and eutectic austenite matrix of sample at Potential 2 (0.758 V vs. SCE) in a pH 14 solution is shown in Fig. 9. In general, the intensity values for all the elements are significantly lower in the case of the specimen exposed at 0.758 V vs. SCE than the one that was held at Potential 1. The lower intensity for chromium in both the cases in relation to iron indicates the fact that Cr being unstable in highly alkaline solution is low in the carbides leaving the corroded region rich in FeO. The significant drop of intensity values of chromium at Potential 2 is due to dissolution of carbides. The study conducted by Varmaa et al. [3] on hardfacing alloys in alkaline solution also showed that when chromium carbides dissolve, chromium element is significantly reduced. The superimposed $\text{Cr}_7\text{C}_3\text{-Fe}$ Pourbaix diagram of Fig. 1 also shows that Potential 2 is in the corrosion region consisting of CrO_4^{2-} and FeO_4^{2-} . Hence, the low levels of chromium.

In summary, it can be said that during oxide film formation in carbides, FeO dominates as iron is the more stable element in carbides in a pH14 solution.

The studies done on microstructure, EIS and ToF-SIMS show that sample at Potential 1 (0.157 V vs. SCE) formed thicker and stable film of FeO on carbide. In any case, the formation of FeO on carbides is itself a result of dissociation of chromium carbide. Further, a passive film from chromium in stainless steels forms due to chromium being distributed as a solute in steel matrix [35] and chromium is not in a combined form as it is in chromium carbide. Hence, it is proposed that although there may be some film on the carbide, dissociation of carbides on the surface is required to form the film. This renders the hardfacing alloy a less effective wear-resistant material when pH 14 solutions are involved in wear applications. In applications involving wear and corrosion, the passive layer may be removed by abrasive particles resulting in further corrosion. It is possible that corrosion dominates the erosion–corrosion mechanism. The study also reveals that FeO dominates over CrO on eutectic austenite matrix and this was also found by Salasi et al. [8].

A possible remedy for mitigating corrosion would be to place the HCWI in the “immune” region as shown in Pourbaix diagram in Fig. 1. The stability of carbides at cathodic potentials (CP) may also be affected by formation of methane gas when hydrogen combines with carbon as shown in Fig. 10. Carbon Pourbaix diagram is superimposed on the Chromium carbide–Iron Pourbaix diagram and this shows a stable region of methane at these potentials. Further investigation is necessary to ascertain the effect of applying cathodic potentials.

Fig. 10 Pourbaix diagram of $\text{Cr}_7\text{C}_3\text{-Fe-C}$ in pH 14 with Potentials 1 and 2 of 9E sample [3, 17, 36]



Another remedy could be adding nitrogen to hardfacing alloys to form nitrides or carbo-nitrides which are likely to provide a good combination of hardness and corrosion resistance [37, 38]. The experimental work is being carried under in our laboratory to add nitrogen as a shielding gas in Gas Metal Arc Welding process.

4 Conclusions

The microstructural, EIS and ToF-SIMS analysis of a chromium carbide-based hardfacing alloy was investigated at Potentials 1 and 2 in pH 14 solution.

- Optical microstructures consisted of primary carbides and eutectic carbides and austenite. XRD analysis identified the carbides to be Cr_7C_3 and Cr_3C_2 and another phase identified was austenite.
- ToF-SIMS showed that a thicker FeO film forms on the primary carbide. CrO layers were thin on both chromium carbide and eutectic austenite. EIS studies showed that at Potential 1 (0.157 V vs. SCE) the sample showed high corrosion impedance and this may be due to the formation of a film on the surface of the sample.
- A denser and more uniform FeO film was found on eutectic austenitic.
- The formation of oxide films on carbides could result in the dissociation of chromium carbides and this dissociation could make the hardfacing alloy less effective in an erosion–corrosion application involving pH 14 medium.

Compliance with Ethical Standards

Conflict of interest The authors declare that they have no conflict of interest.

References

- McLeod A, Clegg RE, Coleman C (2012) Corrosion resistance of white cast irons in caustic solutions. In: Rosenberg S (ed) Proceedings of the 9th International Alumina Quality Workshop. AQW Inc, Brisbane, pp 166–170
- Nelson GD (2010) The influence of microstructure on the corrosion and wear mechanisms of high chromium white irons in highly caustic solutions. PhD Thesis, The University of Adelaide, School of Mechanical Engineering, Australia
- Marimuthu V, Kannoopatti K (2016) Corrosion behaviour of high-chromium white iron hardfacing alloys in an alkaline solution. *J Bio Tribo Corros* 2(4):1–14
- El-Aziz KA, Zohdy K, Saber D, Sallam H (2015) Wear and corrosion behavior of high-Cr white cast iron alloys in different corrosive media. *J Bio Tri Corros* 1(4):1–12
- Salasi M (2012) Synergism Between Abrasion and Corrosion. PhD Thesis, The University of Western Australia, Crawley
- Gou J, Wang Y, Li X, Zhou F (2017) Effect of rare earth oxide nano-additives on the corrosion behavior of Fe-based hardfacing alloys in acid, near-neutral and alkaline 3.5 wt% NaCl solutions. *Appl Surf Sci* 15:431–451
- Krishnan R (2015) Analysing corrosion resistance of hardfacing alloys using electrochemical impedance spectroscopy (EIS). Thesis—the degree of Bachelor of Engineering, Charles Darwin University, Darwin
- Salasi M, Stachowiak G, Stachowiak G, Kilburn M (2013) Nano-SIMS investigation of passive oxide films on high-Cr cast iron. *Corros Sci* 67:298–303

9. Olsson CO, Landolt D (2003) Passive films on stainless steels—chemistry, structure and growth. *Electrochim Acta* 48(9):1093–1104
10. Fajardo S, Bastidas D, Ryan M, Criado M, McPhail D, Bastidas J (2010) Low-nickel stainless steel passive film in simulated concrete pore solution: a SIMS study. *Appl Surf Sci* 256(21):6139–6143
11. Freire L, Catarino M, Godinho M, Ferreira M, Ferreira M, Simões A, Montemor M (2012) Electrochemical and analytical investigation of passive films formed on stainless steels in alkaline media. *Cement Concr Compos* 34(9):1075–1081
12. Freire L, Carmezim M, Ferreira M, Montemor M (2010) The passive behaviour of AISI 316 in alkaline media and the effect of pH: a combined electrochemical and analytical study. *Electrochim Acta* 55(21):6174–6181
13. AS/NZS (2005) AS/NZS 2576:2005, welding consumables for build-up and wear resistance. Australian Standards, Sydney
14. AWRA (1979) AWRA technical note 4: Hardfacing. Australian Welding Research Association, Sydney
15. Borle SD (2014) Microstructural characterization of chromium carbide overlays and a study of alternative welding processes for industrial wear applications. Thesis—Master of Science in Welding Engineering. University of Alberta, Edmonton Alberta
16. Standard ASTM. (2011) G5-94 standard reference test method for making potentiostatic and potentiodynamic anodic polarization measurements. *Ann Book ASTM Stand* 3(2):47–58
17. Marimuthu V, Dulac I, Kannoopatti K (2016) Significance of Pourbaix diagrams to study the corrosion behaviour of Hardfacing alloys based on chromium carbides at 298 K (25 C). *J Bio Tribo Corros* 2(3):1–7
18. Anijdan SM, Bahrami A, Varahram N, Davami P (2007) Effects of tungsten on erosion–corrosion behavior of high chromium white cast iron. *Mater Sci Eng A* 454:623–628
19. Lazić V, Milosavljević D, Aleksandrović S, Marinković P, Bogdanović G, Nedeljković B, Carbide type influence on tribological properties of hard faced steel layer—part I—theoretical considerations. *Tribol Ind* 32(2):11–20
20. Seetharaman S (2013) Treatise on process metallurgy, volume 3: industrial processes, Newnes, Oxford
21. Kayser FX (1996) A Re-examination of westbrook’s X-ray diffraction pattern for Cr₇C₃. *Mater Res Bull* 31(6):635–638
22. ASTM E975-13 (2013) Standard practice for X-ray determination of retained austenite in steel with near random crystallographic orientation. ASTM International, West Conshohocken
23. Deepa P, Padmalatha R (2017) Corrosion behaviour of 6063 aluminium alloy in acidic and in alkaline media. *Arab J Chem* 10:S2234–S2244
24. Dinodi N, Shetty AN (2013) Electrochemical investigations on the corrosion behaviour of magnesium alloy ZE41 in a combined medium of chloride and sulphate. *J Magnes Alloys* 1(3):201–209
25. Morad M (1999) Influence of propargyl alcohol on the corrosion behaviour of mild steel in H₃PO₄ solutions. *Mater Chem Phys* 60(2):188–195
26. Mahato N, Singh M (2011) Investigation of passive film properties and pitting resistance of AISI 316 in aqueous ethanoic acid containing chloride ions using electrochemical impedance spectroscopy (EIS). *Portugaliae Electrochim Acta* 29(4):233–251
27. Burstein G, Cinderey R (1991) The potential of freshly generated metal surfaces determined from the guillotined electrode—a new technique. *Corros Sci* 32(11):1195–1211
28. Cinderey R, Burstein G (1992) The repassivation potential of aluminium in water. *Corros Sci* 33(3):499–502
29. Lin CC, Chang KL, Shih HC (2007) Corrosive behavior of chromium carbide-based films formed on steel using a filtered cathodic vacuum arc system. *Appl Surf Sci* 253(11):5011–5016
30. Zhang X, Shoesmith DW (2013) Influence of temperature on passive film properties on Ni–Cr–Mo Alloy C-2000. *Corros Sci* 76:424–431
31. Zhang X, Zagidulin D, Shoesmith DW (2013) Characterization of film properties on the Ni Cr Mo Alloy C-2000. *Electrochim Acta* 89:814–822
32. Haupt S, Strehblow HH (1995) A combined surface analytical and electrochemical study of the formation of passive layers on FeCr alloys in 0.5 M H₂SO₄. *Corros Sci* 37(1):43–54
33. Hoppe HW, Haupt S, Strehblow HH (1994) Combined surface analytical and electrochemical study of the formation of passive layers on Fe/Cr alloys in 1 M NaOH. *Surf Interface Anal* 21(8):514–525
34. McLeod A, Clegg RE (2013) Effect of exposure time on the morphology of corrosion on high chromium white cast iron in high temperature caustic solutions. *Mater Corr* 64(5):381–387
35. McCafferty E (2010) Introduction to corrosion science. Springer, New York, pp 249–252
36. Schweitzer GK, Pesterfield LL (2010), The aqueous chemistry of the elements. Oxford University Press, Oxford
37. Smith RT (2015) Development of a nitrogen-modified Stainless steel hardfacing alloy. PhD Thesis. The Ohio State University, Columbus
38. Yang K (2015) Corrosion resistance of nitrogen-alloying hardfacing alloy. *J Mater Eng* 43(5):33–37